An open conformation of mammalian cytochrome P450 2B4 at 1.6-Å resolution

Emily E. Scott*†, You Ai He*, Michael R. Wester‡, Mark A. White§, Christopher C. Chin§, James R. Halpert*, Eric F. Johnson‡, and C. David Stout†¶

*Department of Pharmacology and Toxicology, University of Texas Medical Branch, Galveston, TX 77555-1031; Departments of ‡Molecular and Experimental Medicine, MEM-255, and ¶Molecular Biology, MB-8, The Scripps Research Institute, La Jolla, CA 92037; and §Sealy Center for Structural Biology, University of Texas Medical Branch, Galveston, TX 77555-0647

Edited by Minor J. Coon, University of Michigan Medical School, Ann Arbor, MI, and approved August 27, 2003 (received for review June 26, 2003)

The xenobiotic metabolizing cytochromes P450 (P450s) are among the most versatile biological catalysts known, but knowledge of the structural basis for their broad substrate specificity has been limited. P450 2B4 has been frequently used as an experimental model for biochemical and biophysical studies of these membrane proteins. A 1.6-Å crystal structure of P450 2B4 reveals a large open cleft that extends from the protein surface directly to the heme iron between the α-helical and β-sheet domains without perturbing the overall P450 fold. This cleft is primarily formed by helices B′ to C and F to G. The conformation of these regions is dramatically different from that of the other structurally defined mammalian P450, 2C5/3LVdH, in which the F to G and B′ to C regions encapsulate one side of the active site to produce a closed form of the enzyme. The open conformation of 2B4 is trapped by reversible formation of a homodimer in which the residues between helices F and G of one molecule partially fill the open cleft of a symmetry-related molecule, and an intermolecular coordinate bond occurs between H226 and the heme iron. This dimer is observed both in solution and in the crystal. Differences between the structures of 2C5 and 2B4 suggest that defined regions of xenobiotic metabolizing P450s may adopt a substantial range of energetically accessible conformations without perturbing the overall fold. This conformational flexibility is likely to facilitate substrate access, metabolic versatility, and product egress.

The cytochromes P450 (P450s) are a superfamily of heme-containing monooxygenases. They are responsible for the metabolism of an unusually wide range of endogenous and exogenous substrates, including synthesis of steroid hormones, bile acids, and cholesterol, and the degradation of steroids, fatty acids, drugs, toxins, and procarcinogens (1). P450s from families 1, 2, and 3 have evolved to convert lipophilic xenobiotics to more polar metabolites readily conjugated by phase II enzymes, and thus targeted for elimination. The stereo- and regiospecificity of metabolite formation by individual xenobiotic metabolizing P450s suggest very specific substrate–enzyme interactions, whereas the range of substrates metabolized suggests an induced fit type of substrate recognition. Understanding the basis for this specific, yet versatile, metabolism by mammalian xenobiotic metabolizing P450s has been limited by the dearth of structural information for these membrane proteins.

In 2000, the first mammalian P450 structure was published (2, 3), that of P450 2C5, which was engineered to delete the single N-terminal transmembrane domain and to mutate a peripheral membrane-binding site. Recent structures of 2C5 bound with the substrates, diclofenac (4) and 4-methyl-*N*-methyl-*N*-(2-phenyl-2*H*-pyrazol-3-yl)benzenesulfonamide (DMZ) (5), indicate that flexible regions of the protein adapt for substrate binding, and that ligands may bind in multiple orientations. The 2C5 structures generally reveal the enzyme closed around these substrates without an obvious route from the solvent to the buried active site. Structures of bacterial P450s, which share the protein fold of mammalian P450s, have suggested two potential routes to the active site. The structures of P450 102 (BM-3), in the absence of substrate (6), and of P450 101 (cam) with large tethered compounds (7), indicate a channel from the surface of the protein near the loop between helices F and G to the active site. In P450 51, a very different 10-Å-wide channel originates beneath the loop between helices B and C and above the heme plane and opens to the active site (8). These two channels are at ≈90° angles to each other. At present, it is unclear whether ligands for mammalian P450s might use one or both of these channels to gain access to the active site, or whether another route exists in membrane-bound P450s.

The current 1.6-Å 2B4 structure reveals a large cleft from the protein surface to the heme iron and defines an open conformation for mammalian P450s. This cleft is generated by repositioning conserved secondary structure elements in one quadrant of the protein, compared with the 2C5 closed structure. This structure is the highest resolution mammalian P450 structure to date and, to our knowledge, the first experimental structure of a P450 from the 2B subfamily. P450 2B4 is one of the best studied mammalian xenobiotic metabolizing P450s. Coon *et al.* (9) first reported the isolation of 2B4, originally named LM2, from phenobarbital-induced rabbit liver microsomes in 1973. Since that time, 2B4 has served as an experimental model for biochemical and biophysical studies of mammalian P450 interactions with lipid (10–12) and the redox partners NADPH-P450 reductase and cytochrome b_5 (13), as well as mechanistic studies (14–16). Many of these studies, and the extraordinary wealth of site-directed mutagenesis data (17), suggest that a closed conformation would be most compatible with metabolism once substrate is bound in the active site. A dimer of 2B4 in the open conformation is reversible to the catalytically active form in solution, suggesting that dynamic structural changes might occur that would sequentially accommodate substrate access, redox partner binding, catalysis, and product egress. In combination, the structural and functional data suggest that conformational flexibility may be central to the ability of family 2 P450s to bind such a diverse array of xenobiotics.

Methods

Protein Design, Purification, Crystal Growth, and Data Collection. P450 2B4dH differs from the wild-type protein by truncation of the N-terminal transmembrane domain (Δ3–21), mutation of N-terminal residues (E2A, G22K, H23K, P24T, K25S, A26S, H27K, and R29K), and addition of a 4× His tag at the C terminus and metabolizes 7-ethoxy-4-trifluoromethylcoumarin

This paper was submitted directly (Track II) to the PNAS office.

Abbreviations: P450, cytochrome P450; SRS, substrate recognition site.

Data deposition: The atomic coordinates and structure factors have been deposited in the Protein Data Bank, www.rcsb.org (PDB ID code 1PO5).

See Commentary on page 13121.

†To whom correspondence should be addressed at: Department of Pharmacology and Toxicology, University of Texas Medical Branch, 301 University Boulevard, Galveston, TX 77555-1031. E-mail: eescott@x-ray.utmb.edu or dave@scripps.edu.

Table 1. Summary of crystallographic statistics

Crystal	
Construct	2B4dH
Space group	$C222_1$
Unit cell, Å (*a*, *b*, *c*)	57.09/114.20/133.95
Data collection	
SSRL beamline	9–2
Wavelength, Å	0.98
Resolution range, Å	21.7–1.6
Total/unique observations	197,894/57,717
Completeness,* %	99.5 (98.8)
Average I/σ_I*	11.4 (2.1)
Multiplicity*	3.4 (3.0)
R_{sym}*	0.058 (0.591)
Refinement statistics	
R factor, %	21.7
R_{free}, 10% of data	28.9
rms deviation	
Bonds, Å	0.008
Angles, °	2.0
Model statistics	
No. of atoms	4,037
Average B factors, Å^2	
Protein	31.1
Heme	15.5

*Values for the highest-resolution shell are in parentheses.

(7-EFC) in a lipid-independent manner (18). P450 2B4dH was expressed as described (18), with an induction period of 48 h. Isolation from membranes and purification by using Cymal-5 and Ni^{2+} affinity and CM-Sepharose chromatography were essentially as described (19). This protocol was altered by adding 4.8 mM Cymal-5 to the buffer for P450 extraction from membranes and maintaining this detergent throughout Ni^{2+} affinity chromatography. P450 2B4dH was concentrated to >0.60 mM by using a centrifugal device.

Crystals were grown by sitting drop vapor diffusion. The initial 4-μl drops contained 0.28 mM P450, 2.4 mM Cymal-5, 7.5% ethanol, 50 mM sodium citrate, pH 5.5, 25 mM potassium phosphate, pH 7.4, 250 mM NaCl, 0.5 mM EDTA, 0.1 mM DTT, and 10% glycerol. Drops were equilibrated against 0.75 ml of 15% ethanol and 0.1 M sodium citrate, pH 5.5, at 18°C. Macroseeding was required to obtain single crystals of suitable size. The seeded drops were as described above, except that the protein concentration was 0.18 mM, and glycerol was added to the mother liquor (2%) and increased to 11% in the drop. Drops were equilibrated overnight before seeding. The result was single crystals up to 1 mm in length. Matrix-assisted laser desorption/ionization MS on dissolved crystals revealed a molecular mass of 53.7 kDa, corresponding to the predicted protein size.

In preparation for data collection, crystals were briefly flooded with mother liquor containing 30% glycerol and flash-cooled in liquid N_2. Initial data were collected to 2.5 Å by using a Bruker M06-HX22 x-ray generator and a Smart 2k charge-coupled device (CCD) area detector. Data were recorded over 280° (0.2° oscillations, 5-min exposure, at 100 K) and processed by using PROTEUM (20). High-resolution data were collected to 1.6 Å on a single crystal by using beamline 9-2 of the Stanford Synchrotron Radiation Laboratory (Stanford, CA). Data were recorded over 90° (1° oscillations, 30-s exposure, at 100 K) by using a Quantum-315 CCD detector (Area Detector Equipment, San Diego) and processed by using the Collaborative Computational Project 4 programs MOSFILM and SCALA (21). X-ray diffraction statistics are shown in Table 1.

Structure Determination and Refinement. The 2B4dH structure was solved by molecular replacement by using the 2.5-Å data and a search model consisting of the complete 2C5/3LVdH structure (PDB ID code 1N6B) with the nonidentical residues truncated at Cβ. Three independent molecular replacement programs [MOLREP, BEAST, and AMORE (21)] yielded consistent solutions. Portions of the 2C5 model, including helices B′ to C and F to G did not fit the experimental density, necessitating their removal from the initial model and manual model building. The program CNS (22) was used for early rounds of refinement with the low-resolution data. First CNS, and later, SHELX (23), were used for refinement of the 1.6-Å data. The Xfit module of XTALVIEW (24) was used for model building into σ_A-weighted $2F_o - F_c$ electron-density maps.

The final model contains 4,037 atoms, including residues 28–492, heme, and 261 water molecules. The crystallographic *R* factor is 21.7% and the R_{free} is 28.9%. Residues in most favored regions of the Ramachandran plot include 86.5% of the structure, with 12.2% in additionally allowed regions, 2.0% in generously allowed regions, and 0.2% in disallowed regions. Three of the residues with generously allowed ϕ-ψ angles are well defined in strong density (V39, S334, and H335). The remaining residues in generously allowed and disallowed regions are located in the loop between helices B′ and C (Y111, V113, A116, and N117) or the β-turn between helix L′ and β_{3-2} (S475 and V480). The chain connectivity is clear for these residues, but the side chains are not well defined. Coordinates have been deposited in the Protein Data Bank (1PO5).

Enzyme Assays. The NADPH-supported metabolism of 7-EFC in the absence of lipid was measured under saturating conditions as reported (18).

Analytical Ultracentrifugation. Sedimentation velocity experiments were performed by using a Beckman XLA instrument at 20°C and 60,000 rpm. For these experiments, P450 2B4dH was purified in the presence of detergent (sodium cholate or Cymal-5), which was removed by washing before chromatographic elution. For purification with sodium cholate, the final conditions were 500 mM potassium phosphate, 20% glycerol, 10 mM 2-mercaptoethanol, 1 mM EDTA (pH 7.4), and 6 μM 2B4dH. For purification with Cymal-5, the final conditions were 50 mM potassium phosphate, 20% glycerol, 1 mM EDTA, 0.2 mM DTT, 500 mM NaCl, pH 7.4, and 6 μM 2B4dH.

Results and Discussion

X-Ray Structure Determination of CYP2B4. The protein engineering strategy developed to obtain diffraction quality crystals of 2C5 was used to identify a 2B enzyme suitable for crystal generation and x-ray diffraction (2, 3). Elimination of the N-terminal transmembrane domain, modification of the N terminus, and addition of a C-terminal 4× His tag converted a series of 2B enzymes (2B1, 2B4, 2B6, and 2B11) from integral membrane proteins that require detergent for dissociation from the lipid bilayer to peripheral ones liberated by using 0.5 M potassium phosphate. The resulting proteins maintained the regio- and stereospecificity of substrate metabolism, but were present in various aggregation states (18). The four truncated 2B enzymes were subjected to numerous modifications in expression and purification in the presence of sodium cholate. The result was the identification of conditions under which 2B4dH is a monodisperse monomer, as determined by analytical ultracentrifugation (data not shown), making this enzyme a candidate for crystallization trials. This protein exhibits an absorbance maximum at 418–419 nm, which is consistent with the low spin form, and has a normal reduced CO difference spectrum. Subsequent application and adaptation of protocols developed for the purification of 2C5 with the detergent Cymal-5 (19) led to protein that

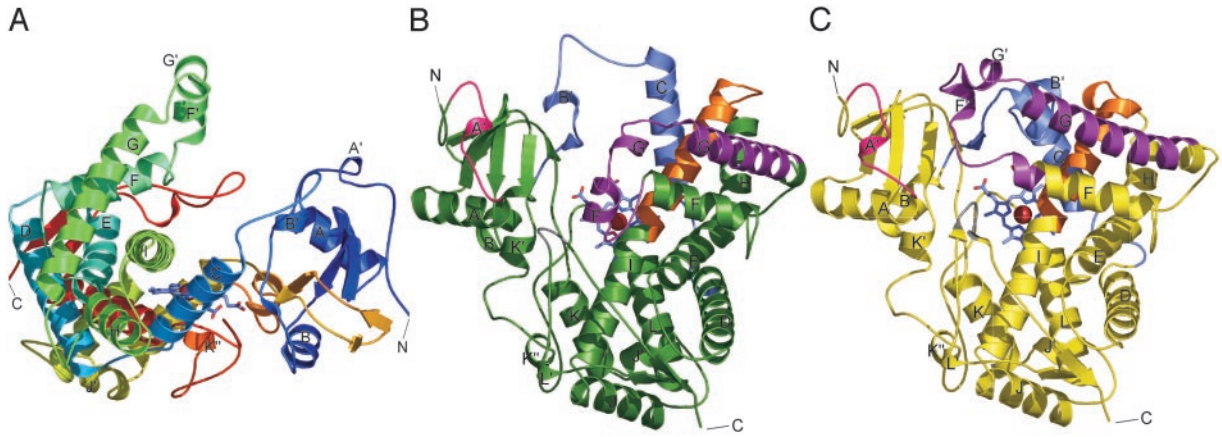

Fig. 1. The 2B4 structure and comparison with 2C5. (*A*) P450 2B4 is oriented to view the large cleft from the protein surface to the heme. The sequence can be traced starting at the blue N terminus and ending at the red C terminus. (B and C) Comparison of 2B4 (*B*) and 2C5/3LV (1N6B) (*C*) structures. Residues with the highest rms deviations between the two structures include 2B4 residues 37–50 (helix A′ and adjacent residues, magenta), residues 92–140 (helix B C terminus to helix D N terminus, blue), residues 206–250 (C-terminal turn of helix F through helix G, purple), residues 275–300 (loop between helices H and I encompassing a three-residue insertion in 2B4 relative to 2C5 and N-terminal half of helix I, orange), and 474–479 (β turn between L′ and β_{3-2}, gray). Excluding these residues, the rms deviation of 324 C^{α} atoms between 2B4 and 2C5 is 1.08 Å. The heme group is shown as a stick figure, and the iron is shown as a red sphere. N and C termini are labeled. Unless otherwise noted, molecular figures were generated by using PYMOL (28).

formed crystals diffracting to 1.6-Å resolution without additional mutations. The structure was solved by using molecular replacement with the 2C5/3LVdH-DMZ structure (5) as a starting model as described in *Methods*. Data collection and refinement statistics are shown in Table 1. Residues in the model are numbered according to the sequence of the full-length protein. Structurally defined residues begin with G28, the first native residue in the truncated form, and continue through the first residue of the C-terminal tag, H492.

Open Cleft from Surface to Active Site. The most significant feature of the 2B4 structure is a large open cleft between the α-helical and β-rich domains that extends from the distal protein surface directly to the heme (Fig. 1*A*). This cleft is ≈15 Å wide and is formed primarily by helices F, F′, G′, and G on one side and by the loop between helices B′ and C and the C helix on the opposing side. Relocation of conserved secondary structures to form the cleft does not disrupt the general architecture of the P450 fold (Fig. 1*B*), which was demonstrated by both soluble bacterial P450s and the mammalian microsomal P450 2C5. An EMBL DALI search (www.ebi.ac.uk/dali) confirmed that the structure of 2B4 is most similar to that of 2C5 (1N6B, Fig. 1*C*), the only other mammalian P450 in the Protein Data Bank. The largest differences between the 2B4 and 2C5 structures are limited to one quadrant of the protein and consist of the helices and loops lining the cleft in 2B4.

The cleft in 2B4 is similar to a 10-Å-wide cleft in the recently reported structure of the bacterial P450 154C1 from *Streptomyces coelicolor A3(2)* (25) (Fig. 2*A*). Both clefts arise from the dissociation of contacts between helix B′ residues and residues in helix G. In contrast to the bacterial enzyme, both 2B4 and 2C5 have an extended number of residues between helices F and G. Although there are differences in the lengths of the F, F′, and G helices between the two mammalian enzymes, the overall secondary structure is maintained. In 2B4, the residues in helices F′ and G′ flex away from helix B′, the core of the protein, and the heme prosthetic group (Fig. 2*B*). In sharp contrast, in 2C5, the same residues interact with helix B′ and the N terminus to form the ceiling of the active site. In addition, helix G rises at a much sharper angle above the active site in 2B4 than in 2C5. As a result, the 2C5 active site is either isolated from or communicates with bulk solvent only via a very narrow channel, depending on the bound ligand. Thus, the 2B4 and 2C5 structures represent dramatically different "open" and "closed" conformations of mammalian P450s.

The opposing side of the 2B4 cleft is formed primarily by helix C and the preceding loop. Again, the secondary structures, in this case helices B′ and C, are retained, but large differences occur in their placement and that of the intervening loop (Fig. 2B). The 2B4 B′ helix, a four-residue 3_{10} helix, is nearly perpendicular to the plane of the heme group, fills the space occupied by helix F′ in the 2C5 structure, and interacts with N-terminal structures. In 2C5 helix B′, a six-residue regular helix, is oriented at an ≈45° angle to the plane of the heme group and interacts with helices G and F′ through a single van der Waals contact to each. The flexible loop between helices B′ and C is extended in both 2C5 and 2B4 and represents one of the regions with the highest B values in the 2B4 structure (79 $Å^2$ for B′-C vs. 31 $Å^2$ for all residues). In the 2B4 open conformation, the angle of helix C shifts in concert with that of helix G, resulting in a much more distal placement for the C helix N terminus compared with 2C5 (Fig. 2*B*). In conjunction with rearrangements in

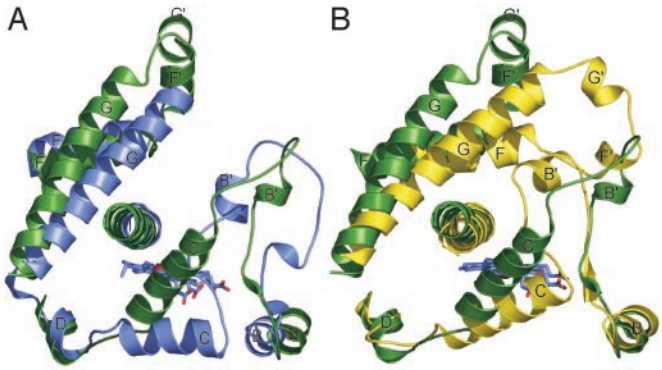

Fig. 2. Comparison of structural elements composing the 2B4 cleft. (*A*) Clefts in the mammalian 2B4 (green) and the bacterial 154C1 (PDB ID code 1GWI, blue) P450s are composed of similar structural elements. (*B*) In 2B4 (green) helices, F′ and G′ flex away from the B′ helix, whereas in 2C5 (yellow), they extend to form the roof of the active site. For clarity, only the regions including helices B through D, F through G, and I are shown. The heme is shown as a stick figure.

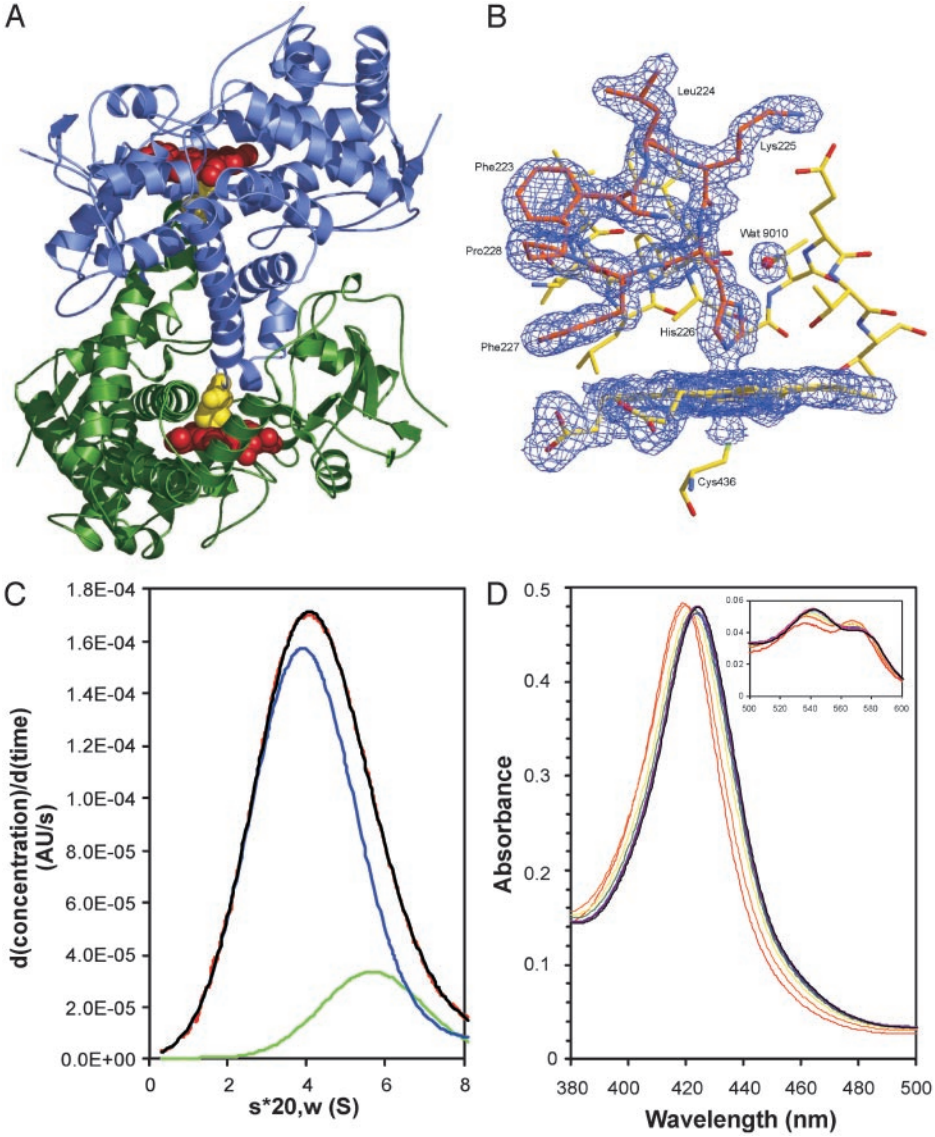

Fig. 3. P450 2B4 dimerization. (*A*) Molecule 2 (blue) of the dimer interacts with molecule 1 (green) through hydrophobic contacts in the helix F to helix G region and coordination of H226 (yellow) to the heme iron (red) of the dimer partner. (*B*) The 2*Fo*−*Fc* omit map contoured at 1 σ shows the interaction of H226 of molecule 2 (CPK coloring with orange carbons) and the iron of molecule 1 (CPK coloring with yellow carbons). The distance from the Fe to the H226 nitrogen is 2.07 Å. A segment of helix I from molecule 1 is shown as a stick model in the background. Figure generated by using XFIT/RASTER3D (24, 29). (*C*) Analytical ultracentrifugation data. At low-protein concentrations (6 μM) 2B4dH purified by using Cymal-5 forms both a monomer and a second species consistent with a dimer. Red line, experimental data; blue, green, and black lines, fitted curves for species 1 (monomer), species 2 (dimer), and the sum of the two species, respectively. (*D*) Shift in Soret absorbance during dimerization. The spectra were recorded for 0.28 mM 2B4dH in the final purification buffer (50 mM potassium phosphate/20% glycerol/1 mM EDTA/0.2 mM DTT/500 mM NaCl, pH 7.4) over the course of 11 h. Corresponding shifts were observed in the α- and β-bands (*Inset*).

the location of residues in helices F′ and G′, this shift of the C helix results in a much greater solvent exposure for the N terminus of helix C in 2B4 than in 2C5 (Fig. 1 *B* vs. *C*).

Dimer Formation in Solution and Crystal. 2B4 crystallizes as a dimer. In the crystal the extended motif composed of helices F′ and G′ of one molecule partially fills the open cleft of a second molecule related by a two-fold crystallographic axis (Fig. 3*A*). Residues 213–230 form close intermolecular hydrophobic interactions, and an intermolecular coordinate bond occurs between H226 and the heme iron. (Fig. 3*B*). Thus, the largely hydrophobic G′ helix, which may be buried in the membrane, associates with the hydrophobic cleft of another molecule to trap the open conformation in the crystalline environment.

The intermolecular histidine-iron coordinate bond provides a convenient spectral reporter of dimerization. Dissolved crystals yield protein with an absorbance maximum at 424 nm, which is typical of ligation between a nitrogen and the iron, and little or no reduced CO difference spectrum. Dilution of dimerized protein to 1–3 μM and addition of 1.2 mM Cymal-5 convert the absorbance maximum to 418 nm, which is indicative of the low spin form, illustrating the reversibility of dimerization. This monomeric 2B4 exhibits a typical Fe^{2+}-CO difference spectrum and oxidizes 7-EFC at 3.4 min^{-1}, a rate identical to that of 2B4 purified in the presence of sodium cholate, which does not form dimers (data not shown). These results demonstrate that the open conformation found in H226-Fe dimers is reversible to a monomeric, catalytically active conformation.

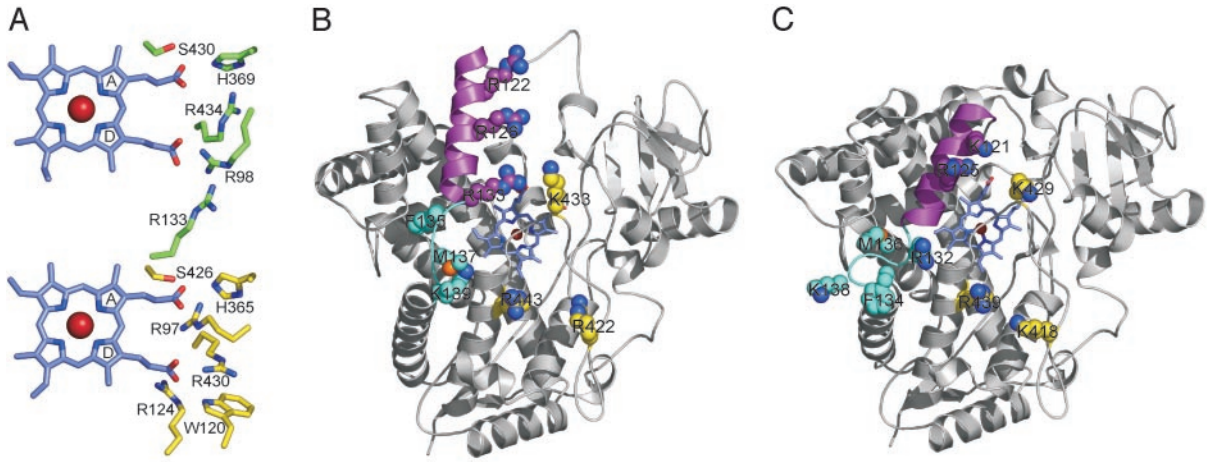

Fig. 4. The location of the C helix affects residues involved in heme ligation and redox partner binding. (*A*) Residues responsible for ligation of the heme propionic acids in 2B4 (*Upper*) and 2C5 (*Lower*). (*B* and *C*) Residues demonstrated by mutagenesis of 2B4 (13) to be involved in reductase and b_5 binding (colored CPK spheres). (*B*) The locations of these residues in the 2B4 open conformation. (*C*) The locations of the corresponding residues in the 2C5 closed conformation. Helix C (purple) and the C to D loop (cyan) are highlighted in *B* and *C*. Numbering of 2B4 residues through Ser-277 is advanced by one number compared with 2C5, due to insertion of a single residue in the N terminus of 2B4. After Ser 277, the 2B4 numbering is advanced by four compared with the 2C5 numbering, due to an additional three-residue insertion between helices H and I. The orientations in *B* and *C* are identical and from the proximal side, a rotation of 180° about the vertical axis from the classical view in Fig. 1 *B* and *C*.

2B4 purified in Cymal-5 also forms the dimer in solution. At low-protein concentrations (6 μM), the Soret maximum is 419–420 nm and analytical ultracentrifugation indicates the formation of a second aggregation state (Fig. 3*C*), which are both consistent with a mixture of monomer and dimer. At protein concentrations equivalent to that in the crystallization setups (0.28 mM), the spectral peak slowly shifts to 424 nm (Fig. 3*D*), which is indicative of H226–Fe interaction in the dimer, with the concomitant loss of the Fe^{2+}–CO complex.

Heme-Binding Site. The spatial orientation of the heme and bracketing helices I and L is strongly conserved, with coordination of iron to the protein through C436. This conserved residue is imperative for generation of activated oxygen at the sixth coordination site on the iron. However, comparison of the 2C5 and 2B4 conformations reveals differences in the interactions between the protein and the heme propionates (Fig. 4*A*). As a result of the shift of helix C compared with the 2C5 and bacterial structures, the propionate of 2B4 heme ring D interacts with helix C residue R133, rather than helix C residues W121 and R125 (corresponding to W120 and R124 in 2C5). In addition, the R98 and R434 side chains (2B4 numbering) reverse roles in the two structures. In 2B4, R98 interacts with the D ring propionate, whereas R434 is located between the two propionate chains. In 2C5, the corresponding R97 residue is between the propionic acids, whereas R430 associates only with the D ring side chain [1N6B, (5)]. Interestingly, each of the residues interacting with the D ring propionate is highly conserved across P450s, except for R133, which is primarily conserved only among the family 2 enzymes. Interactions with the propionate of the heme A ring are conserved between 2B4 (H369 and S430) and the corresponding residues in 2C5 (H365 and S426).

In 2B4, helix I exhibits a distinct bend over the heme group, displacing the N terminus toward the C terminus of helix G (Fig. 2*B*). Smaller bends have been observed in the I helix of liganded structures of 2C5 (4, 5). Larger bends than that in helix I of 2B4 have been observed in azole complexes of bacterial P450s, particularly CYP51 (8). The orientations of the imidazole groups in 4-phenylimidazole bound to CYP51 and in H226 bound to 2B4 differ and may affect the angle of the bend observed in the I helix.

Relationship of Conformation to Redox Partner Binding and Catalysis. The wealth of site-directed mutagenesis data on 2B enzymes in conjunction with the structures of 2C5 and bacterial enzymes suggests that 2B4 also forms a closed conformation. In particular, the location of the C helix in the open conformation of 2B4 alters the likely site for interactions with NADPH-P450 reductase and cytochrome b_5 (13). The proximal surface of P450s generally exhibits a strong positive electrostatic potential in the region of helix C and adjacent to the heme prosthetic group. This electropositive region may interact with the negatively charged surfaces of NADPH-P450 reductase and/or cytochrome b_5, facilitating association and electron transfer. The relocation of helix C in P450 2B4, compared with 2C5, does not substantially reduce the surface electrostatic potential in this region. However, C helix residues R122 and F126, which have been implicated by site-directed mutagenesis in the association of 2B4 with reductase and/or b_5 (13), are relocated in the open conformation compared with the 2C5 closed conformation (Fig. 4 *B* and *C*). In addition, residues at the C terminus of helix C or between helices C and D implicated in redox partner binding (R133, F135, M137, and K139) form a compact loop in the closed conformation, but extend with the relocation of the C helix in the 2B4 open conformation and may act as a spring or hinge for conformational change. P450 102 is a fusion protein consisting of both a P450 domain and a reductase domain. The structure of P450 102 crystallized with the FMN domain of the reductase bound to the proximal surface places helix C more similar to that observed in the closed conformation of 2C5 (26). This finding suggests that the closed form may interact more favorably with P450 reductase. Because 2B4 is active in the monomeric state, the C helix likely moves back into a position that reflects the more conserved conformation seen in the closed structures.

A more closed conformation of 2B4 would also be much more compatible with a bound ligand simultaneously contacting 2B active-site residues identified by extensive site-directed mutagenesis and that have direct counterparts in the 2C5 active site (17). The 2B4 open conformation places active-site residues in helix I at positions 294, 297, 298, and 302 (SRS 4) and those near β_{1-4} at positions 362, 363, and 367 (SRS 5) in close proximity to the iron such that they would contact prototypical substrates in virtually any reactive orientation (Fig. 1*B*). However, the de-

scribed rearrangements relocate several other key active-site residues identified by site-directed mutagenesis away from the heme and away from each other in the 2B4 open conformation. These include residues in helix B′ and the loop between helices B′ and C at positions 103, 114, and 115 (SRS 1), between helices F and F′ at positions 206 and 209 (SRS 2), and between β_{4-1} and β_{4-2} at positions 477 and 478 (SRS 6). The result is that a single orientation of bound substrate could not simultaneously contact all of the active-site residues in the open conformation. As an example, site-directed mutagenesis studies of phenylimidazole binding to 2B4 strongly suggested that residues 114 and 294 act in close proximity to each other (27). In contrast to their locations in the 2B4 open conformation, residues corresponding to 114 and 294, as well as the other active-site residues identified by functional analysis, are grouped in close proximity to the heme, and are available for direct substrate interaction in the closed 2C5 structure. Therefore, a conformational change, potentially to a closed conformation similar to that observed for 2C5, would appear to be required to move many of the active-site residues to positions where they would directly contact substrate after it is bound in the active site of 2B4.

Conclusions

The 1.6-Å structure of substrate-free P450 2B4 reveals substantial differences among the xenobiotic-metabolizing mammalian P450s that may reflect the structural flexibility of these enzymes. Compared with the closed 2C5 structures, striking conformational changes in the regions encompassing helices F to G and B′ to C of 2B4 produce a large cleft to the active site. This open conformation would easily allow the diverse range of xenobiotic substrates metabolized by family 2 P450s to access the vicinity of the heme group without the constrictions imposed by a more channel-like entrance. However, site-directed mutagenesis results suggest that a closed conformation, similar to that observed for 2C5, would be more compatible with redox partner binding and substrate turnover. Reversible interconversion of the open conformation and an enzymatically active form of 2B4 likely to adopt a closed conformation suggests that a transition between conformations is energetically accessible. Alternating between an open form and a closed form would facilitate binding of diverse substrates while allowing stereo- and regiospecific metabolism once the substrate was sequestered in the active site.

We thank Jason Yano and Vidyasankar Sundaresan for assistance with molecular replacement, and the staff at the Stanford Synchrotron Radiation Laboratory for assistance with data collection. The Stanford Synchrotron Radiation Laboratory is operated by the U.S. Department of Energy Office of Basic Energy Sciences. The Stanford Synchrotron Radiation Laboratory Biotechnology Program is supported by the National Institutes of Health, the National Center for Research Resources, the Biomedical Technology Program, and the U. S. Department of Energy Office of Biological and Environmental Research. This work was supported by National Institutes of Health Grants GM20674 (to E.E.S.), ES03619 (to J.R.H.), GM31001 (to E.F.J.), GM59229 (to C.D.S.), National Institute of Environmental Health Sciences Center Grant ES06676 (to J.R.H.), and the Sealy and Smith Foundation (M.A.W. and C.C.C.).

1. Rendic, S. (2002) *Drug Metab. Rev.* **34,** 83–448.
2. Cosme, J. & Johnson, E. F. (2000) *J. Biol. Chem.* **275,** 2545–2553.
3. Williams, P. A., Cosme, J., Sridhar, V., Johnson, E. F. & McRee, D. E. (2000) *Mol. Cell* **5,** 121–131.
4. Wester, M. R., Johnson, E. F., Marques-Soares, C., Dijols, S., Dansette, P. M., Mansuy, D. & Stout, C. D. (2003) *Biochemistry* **42,** 9335–9345.
5. Wester, M. R., Johnson, E. F., Marques-Soares, C., Dansette, P., Mansuy, D. & Stout, C. D. (2003) *Biochemistry* **42,** 6370–6379.
6. Li, H. & Poulos, T. L. (1997) *Nat. Struct. Biol.* **4,** 140–146.
7. Dunn, A. R., Dmochowski, I. J., Bilwes, A. M., Gray, H. B. & Crane, B. R. (2001) *Proc. Natl. Acad. Sci. USA* **98,** 12420–12425.
8. Podust, L. M., Poulos, T. L. & Waterman, M. R. (2001) *Proc. Natl. Acad. Sci. USA* **98,** 3068–3073.
9. Coon, M. J., van der Hoeven, T. A., Kaschnitz, R. M. & Strobel, H. W. (1973) *Ann. N.Y. Acad. Sci.* **212,** 449–457.
10. Bayburt, T. H. & Sligar, S. G. (2002) *Proc. Natl. Acad. Sci. USA* **99,** 6725–6730.
11. Shank-Retzlaff, M. L., Raner, G. M., Coon, M. J. & Sligar, S. G. (1998) *Arch. Biochem. Biophys.* **359,** 82–88.
12. French, J. S., Guengerich, F. P. & Coon, M. J. (1980) *J. Biol. Chem.* **255,** 4112–4119.
13. Bridges, A., Gruenke, L., Chang, Y. T., Vakser, I. A., Loew, G. & Waskell, L. (1998) *J. Biol. Chem.* **273,** 17036–17049.
14. Narasimhulu, S., Havran, L. M., Axelsen, P. H. & Winkler, J. D. (1998) *Arch. Biochem. Biophys.* **353,** 228–238.
15. Vaz, A. D. N., Pernecky, S. J., Raner, G. M. & Coon, M. J. (1996) *Proc. Natl. Acad. Sci. USA* **93,** 4644–4648.
16. Coon, M. J., Vaz, A. D. N., McGinnity, D. F. & Peng, H.-M. (1998) *Drug Metab. Dispos.* **26,** 1190–1193.
17. Domanski, T. L. & Halpert, J. R. (2001) *Curr. Drug Metab.* **2,** 117–137.
18. Scott, E. E., Spatzenegger, M. & Halpert, J. R. (2001) *Arch. Biochem. Biophys.* **395,** 57–68.
19. Wester, M. R., Stout, C. D. & Johnson, E. F. (2002) *Methods Enzymol.* **357,** 73–79.
20. Bruker AXS (2003) PROTEUM (Bruker AXS, Madison, WI).
21. Collaborative Computational Project 4 (1994) *Acta Crystallogr. D* **50,** 760–776.
22. Brunger, A. T., Adams, P. D., Clore, G. M., Delano, W. L., Gros, P., Gross-Kunsleve, R. W., Jiang, J. S., Kuszewski, J., Nilges, N., Pannu, N. S., *et al.* (1998) *Acta Crystallogr. D* **64,** 905–921.
23. Sheldrick, G. M. (1990) *Acta Crystallogr. A* **46,** 467–473.
24. McRee, D. E. (1999) *J. Struct. Biol.* **125,** 156–165.
25. Podust, L. M., Kim, Y., Arase, M., Neely, B. A., Beck, B. J., Bach, H., Sherman, D. H., Lamb, D. C., Kelly, S. L. & Waterman, M. R. (2003) *J. Biol. Chem.* **278,** 12214–12221.
26. Sevrioukova, I. F., Li, H., Zhang, H., Peterson, J. A. & Poulos, T. L. (1999) *Proc. Natl. Acad. Sci. USA* **96,** 1863–1868.
27. Spatzenegger, M., Wang, Q., He, Y. Q., Wester, M. R., Johnson, E. F. & Halpert, J. R. (2001) *Mol. Pharmacol.* **59,** 475–485.
28. Delano, W. L. (2003) *PyMOL Users Manual* (DeLano Scientific, San Carlos, CA).
29. Merritt, E. A. & Bacon, D. J. (1997) *Methods Enzymol.* **277,** 505–524.